Intercomparison of the Southern Ocean Circulations in IPCC Coupled Model Control Simulations

JOELLEN L. RUSSELL

Atmospheric and Oceanic Sciences, Princeton University, Princeton, New Jersey

RONALD J. STOUFFER AND KEITH W. DIXON

NOAA/GFDL, Princeton, New Jersey

(Manuscript received 4 May 2005, in final form 29 November 2005)

ABSTRACT

The analyses presented here focus on the Southern Ocean as simulated in a set of global coupled climate model control experiments conducted by several international climate modeling groups. Dominated by the Antarctic Circumpolar Current (ACC), the vast Southern Ocean can influence large-scale surface climate features on various time scales. Its climatic relevance stems in part from it being the region where most of the transformation of the World Ocean's water masses occurs. In climate change experiments that simulate greenhouse gas–induced warming, Southern Ocean air–sea heat fluxes and three-dimensional circulation patterns make it a region where much of the future oceanic heat storage takes place, though the magnitude of that heat storage is one of the larger sources of uncertainty associated with the transient climate response in such model projections. Factors such as the Southern Ocean's wind forcing, heat, and salt budgets are linked to the structure and transport of the ACC in ways that have not been expressed clearly in the literature. These links are explored here in a coupled model context by analyzing a sizable suite of preindustrial control experiments associated with the forthcoming Intergovernmental Panel on Climate Change's Fourth Assessment Report. A framework is developed that uses measures of coupled model simulation characteristics, primarily those related to the Southern Ocean wind forcing and water mass properties, to allow one to categorize, and to some extent predict, which models do better or worse at simulating the Southern Ocean and why. Hopefully, this framework will also lead to increased understanding of the ocean's response to climate changes.

1. Introduction

Recently, an unprecedented effort has been made by climate modeling groups to provide climate model results to the international climate research community. This effort is in support of the Intergovernmental Panel on Climate Change's Fourth Assessment Report (IPCC AR4). As part of the IPCC-requested standard set of integrations, sets of control integrations, idealized forcing experiments, simulations of the past 100+ years, and multiple projections of future climate scenarios are performed. This analysis focuses on an evaluation of the Southern Ocean simulation in the preindustrial control integrations (Picntrl in the IPCC AR4 nomenclature) of a set of atmosphere–ocean–land surface–sea ice global coupled climate models developed by several international modeling groups.

The ability of IPCC class climate models to simulate the Southern Ocean circulation is important, since it is a part of the coupled climate system that plays an important role in the global carbon cycle and surface climate change patterns. It has been shown in earlier papers (e.g., Manabe et al. 1991; Cubasch et al. 2001) that the Southern Ocean is a region of minimum warming as greenhouse gases (GHGs) increase in the atmosphere. It is also a region where most of the oceanic heat storage is projected to occur (Sarmiento et al. 1998). The oceanic heat storage is one of the larger sources of uncertainty in both historical estimates (Gregory et al. 2004) and future climate change projections (Cubasch et al. 2001).

The Southern Ocean circulation is dominated by the Antarctic Circumpolar Current (ACC). This current

Corresponding author address: Dr. J. L. Russell, Department of Geosciences, University of Arizona, 1040 E. Fourth St., Tucson, AZ 85721.
E-mail: jrussell@geo.arizona.edu

transports about 135 Sverdrups (1 Sv $\equiv 10^6$ m^3 s^{-1}) of water around Antarctica (Cunningham et al. 2003; García et al. 2002) with a range among the observational estimates of about 10%. The maximum flow of the current is normally concentrated in two roughly parallel fronts, the Subantarctic Front and the Polar Front, with the Polar Front being closer to the Antarctic continent. The Ekman drift in the surface layer is substantial, as a result of the strength of the westerly winds over the Southern Ocean. This northward drift of the surface waters creates a divergence south of the Polar Front, which creates vast areas of upwelling water (Peterson and Whitworth 1989). Precipitation tends to accumulate in the surface waters during their drift northward, lowering the salinity of the water. Southern Ocean surface waters subduct across the fronts forming Subantarctic Mode Water (SAMW) and Antarctic Intermediate Water (AAIW), the building blocks of the global ocean shallow-overturning circulation (Talley 2003).

The mechanisms by which winds drive the ACC have been the subject of extensive debate over the past 50 years. Munk and Palmen (1951) first suggested that the surface wind stress over the ACC might be balanced by form stress due to pressure gradients across topographic obstructions on the ocean floor. The momentum balances in some ocean-only numerical models of the Southern Ocean are consistent with wind stress balancing form stress (Stevens and Ivchenko 1997; Gille 1997), but in their simplest form do not account for the strength of the mean ACC. As an alternative to the direct forcing mechanism, Stommel (1957) pointed out that wind stress curl might drive the ACC in a fashion similar to midlatitude Sverdrup dynamics. More recent studies based on ocean-only numerical models have suggested that in addition to wind stress and wind stress curl, buoyancy forcing may also play a role in determining ACC transport (Gnanadesikan and Hallberg 2000; Gent et al. 2001). Available data are inadequate to provide definitive explanations for the dynamical processes controlling the mean flow of the ACC, since study of the mean ACC would require not only the mean transport, but also how it would differ under alternative ocean conditions.

The Southern Ocean water mass distribution and circulation is particularly sensitive in two ways to the strength and position of the westerly winds. First, the position of the westerlies relative to the topography in the poleward-eastern corners of the Pacific and Indian Oceans determines the density of the water subducted to form SAMW (McCartney 1977, 1982) and AAIW (Talley 1996). Second, the position of the westerlies is important because these winds produce a divergent upwelling flow along the southern boundary of the ACC. The water pulled to the surface along isopycnal surfaces by this divergence is relatively warm and salty and comes from great depth (Gordon 1971). A component of this upwelled deep water is entrained into the Ekman layer and advected north toward the Subantarctic Front (Gordon 1971). The formation of Antarctic Bottom Water (AABW) and Circumpolar Deep Water (CDW) are also affected by the surface westerly winds through this entrainment of salt from North Atlantic Deep Water (NADW) pulled into the South Atlantic through the surface divergence.

In addition to the effect of the high-latitude heat flux from the ocean to the atmosphere and the amount of relatively fresh SAMW and AAIW exported north of the ACC, the density gradient across the ACC is determined by the relative amount of salty NADW pulled near the surface from below the sill depth of the Drake Passage south of the ACC. There are three obvious ways a model can get this wrong. 1) If the winds are too strong and the Southern Ocean divergence pulls too much salty water to the surface, then the water column becomes unstable and open-ocean convection homogenizes the polar gyre. 2) If the model's winds are too weak or shifted too far equatorward, then the surface water divergence is weak and the upwelling of salty water is weak. 3) If a model produces too little NADW or the NADW produced is too warm or too fresh, the density gradient across the current cannot be maintained and the ACC transport weakens. We will present evidence that the ability of an ocean model to export salty North Atlantic Deep Water into the Southern Ocean is the most significant internal ocean contribution to the variability between the 18 IPCC AR4 models studied here.

The models chosen for this study are those that had their temperatures, salinities, and velocities (zonal and meridional) reported for the preindustrial control experiment (Picntrl) to the Program for Climate Model Diagnosis and Intercomparison (PCMDI) at Lawrence Livermore National Laboratory (http://www-pcmdi.llnl.gov/). In this experiment, the radiative forcing agents are held constant at preindustrial levels. Typically, these control integrations are used as control for the other perturbation integrations archived at PCMDI. Most of these models also had various other quantities collected at PCMDI: barotropic streamfunction, free-surface elevation, sea ice cover, zonal wind stress, the various terms of the surface heat flux (latent heat, sensible heat, shortwave radiation, and longwave radiation), and the surface freshwater flux. Not all models had all of these quantities archived, so several of the figures presented here may be missing one or more of

the 18 simulations. In all cases, we averaged the last 20 years of each (Picntrl) control simulation to create the annual averages for the variables compared here.

Some documentation of the models is available at the PCMDI Web site given above. If interested, the reader is encouraged to follow those references for a detailed description of any of the models used in this study. For our purposes, it is enough to note that these models represent the present-day state-of-the-art in AOGCMs.

It also needs noting that numerical studies have demonstrated that the magnitude of the eddy-mixing coefficient can greatly impact the strength of the ACC transport (Hasumi 2002). It is likely that the choice of other subgrid-scale parameterizations will also impact the Southern Ocean simulation. Here we focus on the simulation itself and try to develop a framework for characterizing the simulations. It is clear that the type of the subgrid-scale parameterizations and the associated coefficients will impact the simulations. This evaluation is an ongoing research activity.

The analysis framework presented here provides a means to categorize, and to some extent predict, the quality and nature of the different Southern Ocean simulations. This study attempts to increase our understanding of what drives and determines the ACC by identifying certain relationships between the wind stress, wind stress curl, buoyancy forcing, and ACC transport present in a suite of 18 coupled climate models. It also identifies reasons why most of the model-to-model differences exist. However, the analyses fall short of offering a definitive explanation of the ACC dynamics, in part because of the large variations in the model configurations. We have chosen these analyses to explore one particular set of questions designed to improve our understanding of how and why these 18 models' Southern Ocean simulations vary from one another and from observations, using relatively simple model diagnostics and corollary observed ocean data.

2. Antarctic Circumpolar Current transport

Particularly at high latitudes where the ocean is weakly stratified, currents tend to be vertically coherent (or barotropic) because of the earth's rotation. These currents steer around major topographic features, like ridges and seamounts, which they cannot pass through. Since ocean surface currents align in roughly the same direction as deep ocean currents, they tend to follow contours of constant depth, thereby detouring around the bumps and troughs in the seafloor (Schulman 1975). Contours of sea surface height (SSH) and barotropic streamfunctions (Fig. 1) will thus tend to reflect the bottom topography.

Figure 1a shows the observed annually averaged sea surface height from the TOPEX data (Fu et al. 1994). We present this as a proxy for the barotropic streamfunction since the free surface is directly related to the pressure gradient and therefore the barotropic transport. In the Southern Hemisphere, low pressure (blue) drives a clockwise flow around the Antarctic continent. The barotropic streamfunction is presented for each of the IPCC models for which it is available, with the blue shading indicating a clockwise flow and the red shading counterclockwise. For those models that did not report a barotropic streamfunction {Goddard Institute for Space Studies Atmosphere–Ocean Model (GISS-AOM; Fig 1i), GISS-ModelE [Hybrid Coordinate Ocean Model (HYCOM) Ocean; GISS-EH; Fig. 1j], and U.K. Met Office Hadley Centre Global Environmental Model (UKMO-HadGEM1; Fig. 1s)} we present the simulated sea surface height.

All of the models correctly simulate the eastward flow through the Drake Passage (except for the GISS-EH model which has a westward flow at the bottom). The Geophysical Fluid Dynamics Laboratory Climate Model (GFDL-CM2.0; Fig. 1g), GFDL-CM2.1 (Fig. 1h), and Model for Interdisciplinary Research on Climate [MIROC3.2(hires); Fig. 1p] are the only ones within 20% of the estimated observed transport of 135 Sv (see Table 1). Many of the other models have transports within 50 Sv of the observation-based value, although the Commonwealth Scientific and Industrial Research Organisation Mark 3.0 (CSIRO-Mk3.0; Fig. 1f), GISS-ModelE (Russell Ocean; GISS-ER; Fig. 1k), and UKMO Third Hadley Centre Coupled Ocean–Atmosphere GCM (HadCM3; Fig. 1r) are clearly too strong, while the Centre National de Recherches Météorologiques Climate Model (CNRM-CM3; Fig. 1e), Institute for Atmospheric Physics, Flexible Global Ocean Atmosphere Land Systems (IAP-FGOALS1.0; Fig. 1l), and Institut Pierre Simon Laplace CM4 (IPSL-CM4; Fig. 1n) are clearly too weak.

As expected from previous studies, the strength of the ACC scales with both the strength of the maximum wind stress (the barotropic component; Fig. 2a), and the mean density gradient across the current (Fig. 2b). The CSIRO-Mk3.0 simulation has the strongest wind stress [~30% greater than the National Centers for Environmental Prediction (NCEP) long-term mean; Kistler et al. 2001], the largest density gradient, and an unrealistically large transport of over 330 Sv (Table 1). The UKMO-HadCM3 simulation has reasonable winds, but also has an excessive salinity gradient and therefore an overly vigorous ACC. The GISS-EH model on the other hand has the lowest wind stress (~40% less than NCEP) and an unrealistic net west-

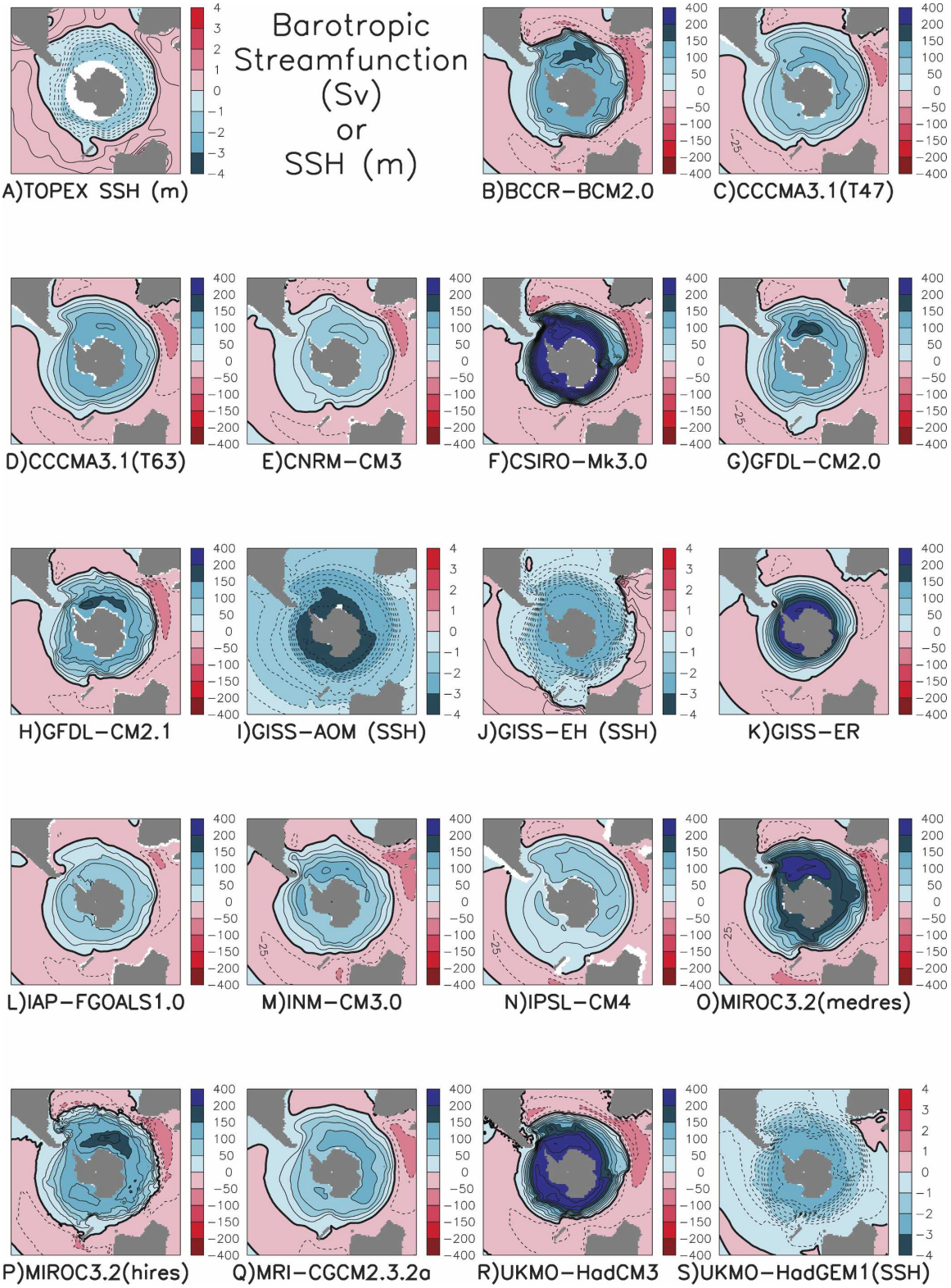

FIG. 1. Free-surface elevation (in m) and barotropic streamfunction (in Sv) from the observations (TOPEX; Fu et al. 1994) and the IPCC ocean simulations. All panels are the barotropic streamfunction, with (a) (k), (l) three exceptions. The streamfunctions for the GISS-AOM, the GISS-EH, and the UKMO-HadGEM1 simulations are currently unavailable.

TABLE 1. Various parameters related to the strength of the ACC. The ACC transport is the integral of the zonal velocity across the Drake Passage at 69°W. The density gradient ($d\rho/dy$) is the zonally averaged density difference between 65° and 45°S. The total ACC-related wind stress (τ_x total) is the integral of the zonal wind stress over the Drake Passage channel (54°–64°S). The maximum westerly wind stress (τmax) is the maximum of the zonally averaged wind stress that is located at the latitude given by Lat τmax. The observed ACC strength is from Cunningham et al. (2003). The observed density gradient is calculated from the *World Ocean Atlas 2001* (Conkright et al. 2002). The observed wind data are from the NCEP long-term mean (Kistler et al. 2001). NA indicates data not archived at PCMDI.

Model	ACC (Sv)	$d\rho/dy$ (kg m^{-3})	Total τ_x 10^{12} N	Max τ_x (N m^{-2})	Lat of max τ_x
Observational estimate	135	0.58	6.5	0.161	52.4
CSIRO-Mk3.0	336	0.85	7.8	0.207	51.3
GISS-ER	266	0.62	4.3	0.107	46.0
UKMO-HadCM3	223	0.97	6.4	0.163	51.3
GISS-AOM	202	0.38	2.9	0.166	43.5
UKMO-HadGEM1	199	0.65	7.1	0.190	52.5
MIROC3.2(medres)	190	0.43	5.3	0.184	46.0
GFDL-CM2.1	135	0.58	6.1	0.162	51.0
MIROC3.2(hires)	125	0.49	6.3	0.175	46.5
GFDL-CM2.0	113	0.56	4.5	0.149	46.0
CCCMA-CGCM3.1(T63)	106	0.43	7.2	0.192	48.8
BCCR-BCM2.0	105	0.53	NA	NA	48.8
MRI-CGCM2.3.2a	94	0.40	5.6	0.157	48.8
CCCMA-CGCM3.1(T47)	93	0.27	5.9	0.180	46.4
INM-CM3.0	80	0.71	6.0	0.172	48.0
IAP-FGOALS1.0g	75	0.39	4.8	0.138	48.8
CNRM-CM3	54	0.31	2.4	0.106	46.0
IPSL-CM4	34	0.18	2.7	0.160	41.8
GISS-EH	−6	0.43	3.6	0.096	46.0

ward flow through the Drake Passage. The complex water mass structure in the Southern Ocean leads to differing effects of the thermal (Fig. 2c) and haline (Fig. 2d) gradients on the strength of the ACC. The models show distinct correlations between the temperature differences and salinity differences between 65° and 45°S and the modeled ACC transport. Several of the models are clustered close to the observed values in all four panels of Fig. 2: GFDL-CM2.1, GFDL-CM2.0, and MIROC3.2(hires) are closest. We will present evidence that the ability of the ocean model component of a global coupled climate model to export salty North Atlantic Deep Water into the Southern Ocean is the most significant *internal* ocean contribution to the intermodel ACC simulation differences.

Various parameters relating to the strength of the ACC that are discussed in this analysis are presented in Table 1. As was seen in Fig. 1 and Fig. 2, the ACC scales with the integral of the wind stress over the Drake Passage latitude band (54°–64°S) as well as the density gradient across the ACC above the sill depth (0–1500 m, 65°–45°S), the temperature gradient, and the salinity gradient. The models that capture the transport most accurately are the GFDL runs and the MIROC (hires) run. Several of the models have ACC transports 20%–40% below the observations. These are the Bjerknes Center for Climate Research (BCCR), the Canadian Centre for Climate Modelling and Analysis (CCCMA), and the Meteorological Research Institute (MRI) simulations. The others have very high or very low flow (more than 40% over or under the observations). On the high side are the CSIRO, GISS-AOM, GISS-ER, MIROC3.2(medres), and the UKMO runs. The CNRM, IAP, Institute for Numerical Mathematics Climate Model (INMCM), and IPSL experiments greatly underestimate the net transport.

3. Surface forcing of the Southern Ocean

The distribution and magnitude of the wind stress over the Southern Ocean compares relatively poorly in most of the AR4 coupled climate models (Fig. 3). The peak zonally averaged wind stress is shifted equatorward in all models (except for UKMO-HadGEM1) relative to the observations (from NCEP long-term mean; Kistler et al. 2001). The best representations in terms of position and strength of the peak westerlies are from the GFDL-CM2.1 and UKMO-HadCM3. The CSIRO simulation is near the observed latitude but its peak is 28% too strong. The HadGEM1 simulation gets the latitude nearly perfectly but is 18% too strong. The peak zonally averaged wind stresses in the CNRM-CM3, GISS-EH, and GISS-ER simulations are 30% weaker than the NCEP long-term mean.

Figure 4 shows the zonally averaged sea surface temperatures (0–100 m), sea surface salinities (0–100 m),

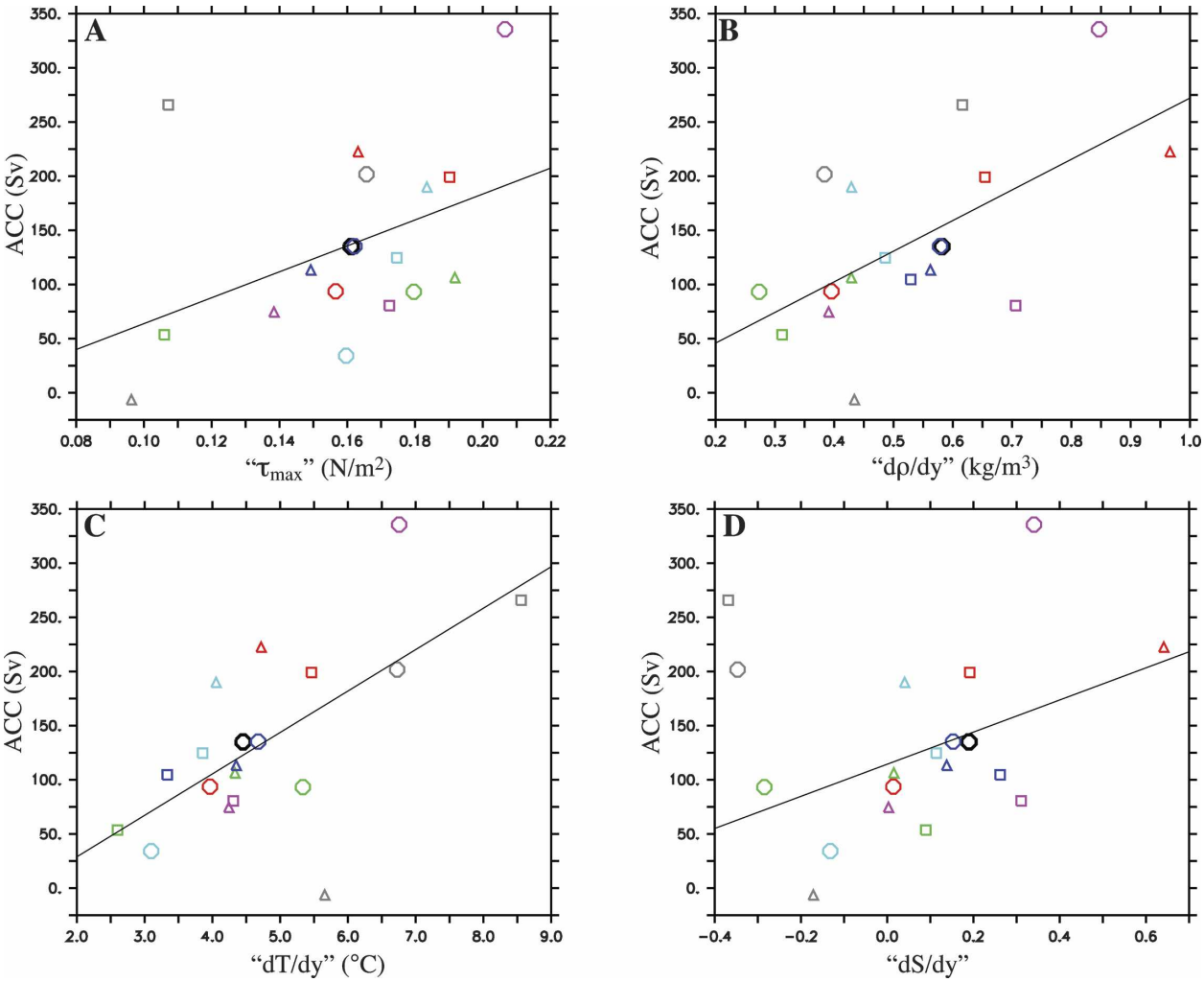

FIG. 2. (a) The maximum wind stress between 70° and 30°S (N/m^2) and the zonally and depth-averaged (0–1500 m) difference in (b) density, (c) temperature, and (d) salinity between 65° and 45°S in each of the IPCC models and the observations, plotted against the ACC transport at Drake Passage (69°W). Observed (black circle), GFDL-CM2.1 (blue circle), GFDL-CM2.0 (blue triangle), BCCR-BCM2.0 (blue square), CCCMA3.1-T47 (green circle), CCCMA3.1-T63 (green triangle), CNRM-CM3 (green square), CSIRO-Mk3.0 (magenta circle), GISS-AOM (gray circle), GISS-EH (gray triangle), GISS-ER (gray square), IAP-FGOALS1.0g (magenta triangle), INM-CM3.0 (magenta square), IPSL-CM4 (cyan circle), MIROC3.2(medres) (cyan triangle), MIROC3.2(hires) (cyan square), MRI-CGCM2.3.2a (red circle), UKMO-HadCM3 (red triangle), and UKMO-HadGEM1 (red square). The black lines are the best linear fit between the two properties. The GISS-ER model has been excluded from the linear fit in (d).

and the heat and freshwater fluxes in the Southern Hemisphere. The model simulations capture the surface temperature distribution reasonably well. The GISS-EH (gray, triangles) simulation is much too warm at high latitudes. The GISS-AOM (gray, circles), GISS-ER (gray, squares), and UKMO-HadCM3 (red, triangles) simulations are several degrees too warm at the equator, while the BCCR-Bergen Climate Model (BCM2.0; blue, squares), CNRM-CM3 (green, squares), GISS-EH (gray, triangles), INM-CM3.0 (magenta, squares), and MRI-CGCM2.3.2a (red, circles) are several degrees too cold.

The simulations show much more variability in their representation of the surface salinity (Fig. 4b). Across the ACC (between 60° and 50°S), most are within a few tenths, but the UKMO-HadCM3 (red, triangles) is much too fresh, and the GISS-EH (gray, triangles) is much too salty. Most of the models underestimate the surface salinity at 35°S; this is likely due to errors in the injection of subtropical salt by excessively weak east Australian and Agulhas currents. The salinity anomalies are also closely linked to the wind curl anomalies; as was previously noted, all of the models have the peak winds (and thus, the zero wind stress curl) too far north-

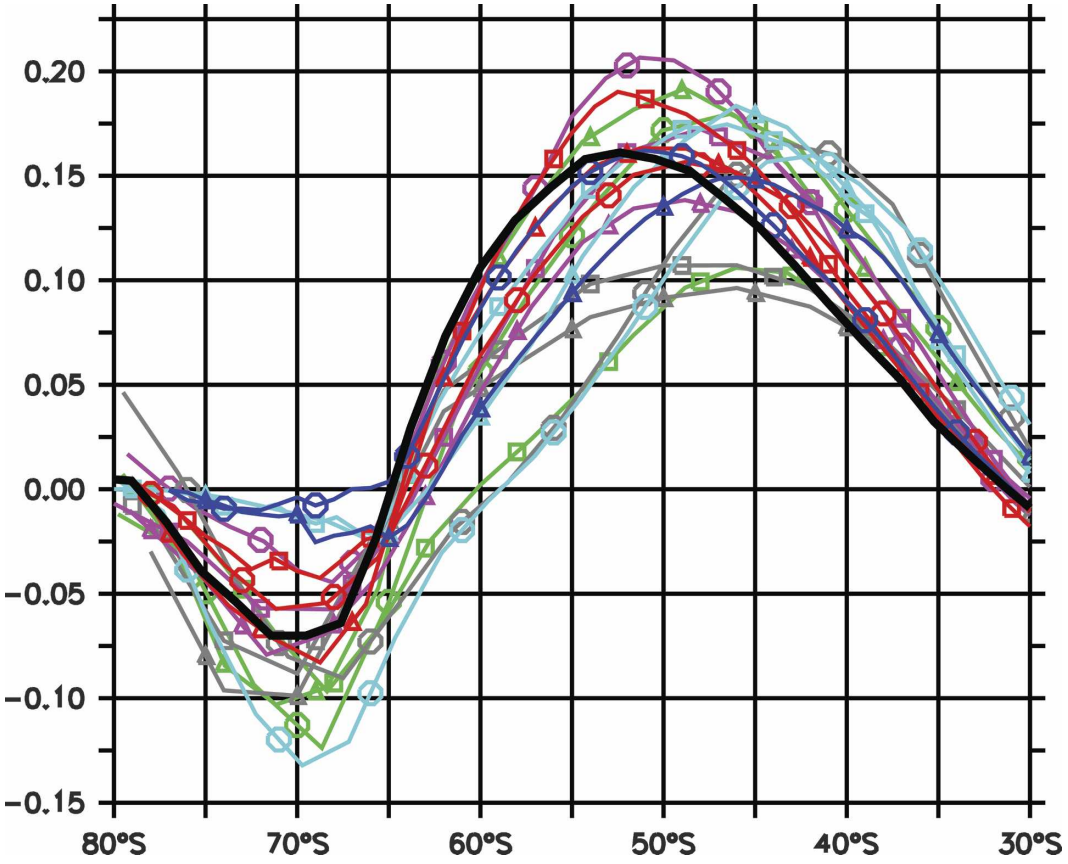

FIG. 3. Zonally averaged wind stress (N m^{-2}). Observed (black), GFDL-CM2.1 (blue circle), GFDL-CM2.0 (blue triangle), CCCMA3.1-T47 (green circle), CCCMA3.1-T63 (green triangle), CNRM-CM3 (green square), CSIRO-Mk3.0 (magenta circle), GISS-AOM (gray circle), GISS-EH (gray triangle), GISS-ER (gray square), IAP-FGOALS1.0g (magenta triangle), INM-CM3.0 (magenta square), IPSL-CM4 (cyan circle), MIROC3.2(medres) (cyan triangle), MIROC3.2(hires) (cyan square), MRI-CGCM2.3.2a (red circle), UKMO-HadCM3 (red triangle), and UKMO-HadGEM1 (red square).

ward by up to 10° of latitude. This alters the divergence at the southern edge of the ACC and thus the upwelling.

Observational estimates of the surface fluxes over the ocean are in general quite uncertain; this is particularly the case in the Southern Ocean. Here we use the da Silva et al. (1994) estimates, however the reader is cautioned to view the comparisons of the observations to model results with some skepticism. Compared to the observational estimates (da Silva et al. 1994), all of the models underestimate the heat loss at 30°S. Most also overestimate the heat loss between 50° and 70°S, except for the BCCR (blue, squares) and IPSL (cyan, circles), which have a net heat input into the ocean at all latitudes north of 70°S. The IAP (magenta, triangles) has an overly positive $E - P$ at 60°S, and the MIROC3.2(hires) (cyan, squares) has several spiky positive features.

4. Water mass simulations

We now present a more detailed analysis of the circulation in the South Atlantic at 32°S. Talley (2003) decomposed the density structure into six classes, representing the Ekman transport, the upper thermocline between the surface and $\sigma_0 = 26.2$, the lower thermocline between 26.2 and 26.9, the AAIW layer between 26.9 and 27.4, the NADW layer between $\sigma_0 = 27.4$ and $\sigma_4 = 45.86$, and AABW between 45.86 and the bottom, and we have done the same type of analysis here. We have subdivided each layer into four sublayers to perform a more detailed analysis. The only technical issue was in dividing the NADW layer into subclasses that do not overlap. We determined that in none of the model simulations was the $\sigma_0 = 27.6$ contour below the $\sigma_4 = 45.86$ contour so Talley's NADW was divided into layers between 27.4 and 27.45, 27.45 and 27.5, 27.5 and 27.6, and 27.6 and 45.86.

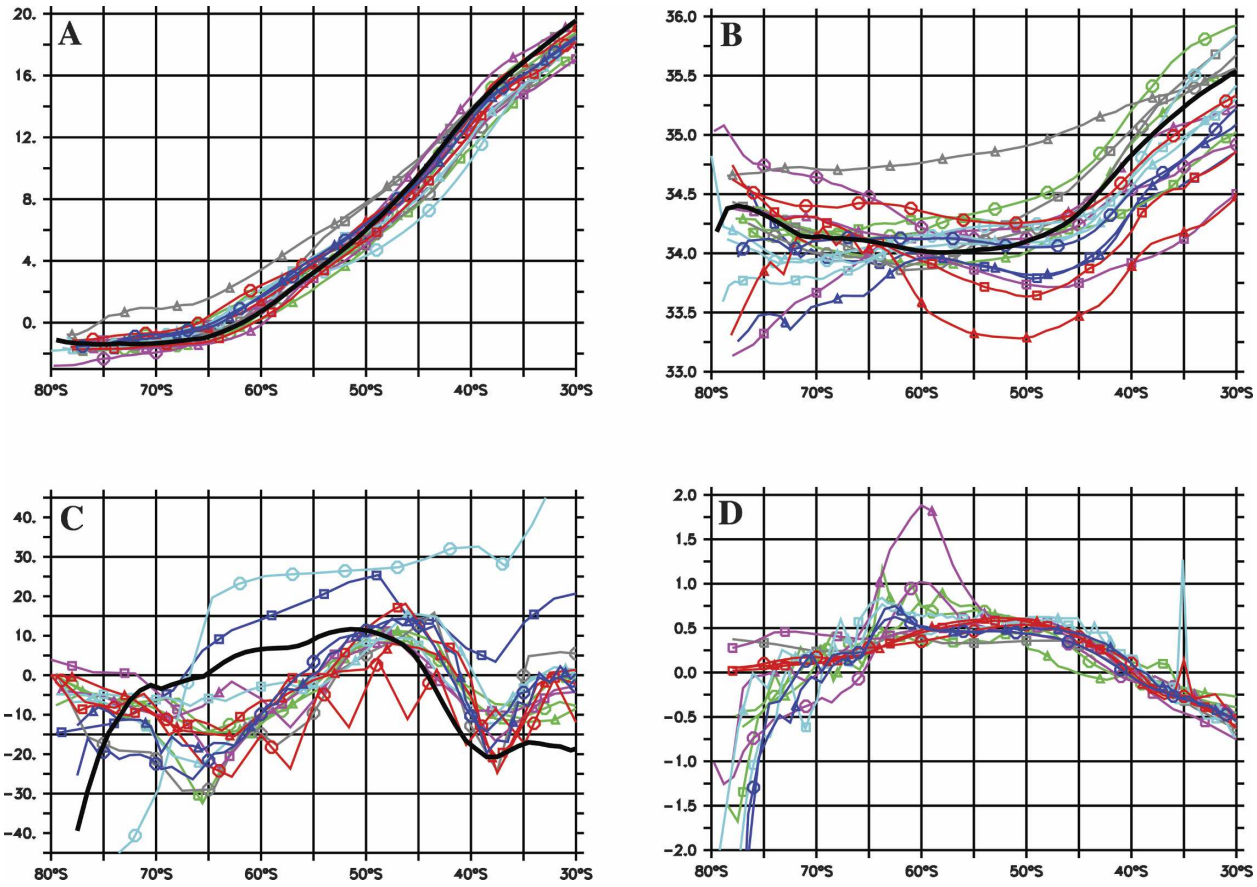

FIG. 4. (a) Zonally averaged sea surface temperature (°C, 0–100-m average) and (b) sea surface salinity (0–100-m average). (c) Zonally averaged surface heat flux in W m^{-2}; (d) zonally averaged freshwater flux in m yr^{-1}. The heat flux is the sum of the latent heat, sensible heat, and downward and upward longwave and shortwave heating at the surface. Observed (black), GFDL-CM2.1 (blue circle), GFDL-CM2.0 (blue triangle), BCCR-BCM2.0 (blue square), CCCMA3.1-T47 (green circle), CCCMA3.1-T63 (green triangle), CNRM-CM3 (green square), CSIRO-Mk3.0 (magenta circle), GISS-AOM (gray circle), GISS-EH (gray triangle), GISS-ER (gray square), IAP-FGOALS1.0g (magenta triangle), INM-CM3.0 (magenta square), IPSL-CM4 (cyan circle), MIROC3.2(medres) (cyan triangle), MIROC3.2(hires) (cyan square), MRI-CGCM2.3.2a (red circle), UKMO-HadCM3 (red triangle), and UKMO-HadGEM1 (red square).

Another issue is one of climate drift in the models. If a model suffers a large amount of climate drift, its density structure may be quite different from the observed density structure. Climate drift then could lead to a miscategorization of the flows using the Talley method. An examination of the currents in the model suggests that this problem is not the primary reason for the model errors outlined below, however, the reader should bear this problem in mind when evaluating the model results. As additional caveat, transports calculated from model output from non-*Z*-coordinate models or from models with non-Cartesian grids may produce less accurate representations of the models than for model output that did not require remapping for submission to PCMDI.

Talley (2003) determined that the southward flow of 17.8 Sv of NADW is balanced by northward flows in the other layers (Fig. 5a). The BCCR-BCM2.0 (Fig. 5b), CSIRO-Mk3.0 (Fig. 5f), GFDL-CM2.0 (Fig. 5g), GFDL-CM2.1 (Fig. 5h), and MIROC3.2(medres) (Fig. 5o) simulations are the most realistic (17.8 Sv ± 20% or 3.6 Sv), although there are sizeable errors in many density ranges. The INM-CM3.0 (Fig. 5m) run has excessive transport in the NADW layer, which is also too warm and too salty. The CCCMA-T63 (Fig. 5d), GISS-AOM (Fig. 5i), GISS-ER (Fig. 5k), IAP-FGOALS1.0g (Fig. 5l), MIROC3.2(hires) (Fig. 5p), UKMO-HadCM3 (Fig. 5r), and UKMO-HadGEM1 (Fig. 5s) experiments are weak, but the flows seem to be slightly offset from their observed density class. The other models all have extremely weak integrated NADW density flow implying that the North Atlantic overturning in these models does not contribute significantly to the density gradient across the ACC in the Southern Ocean.

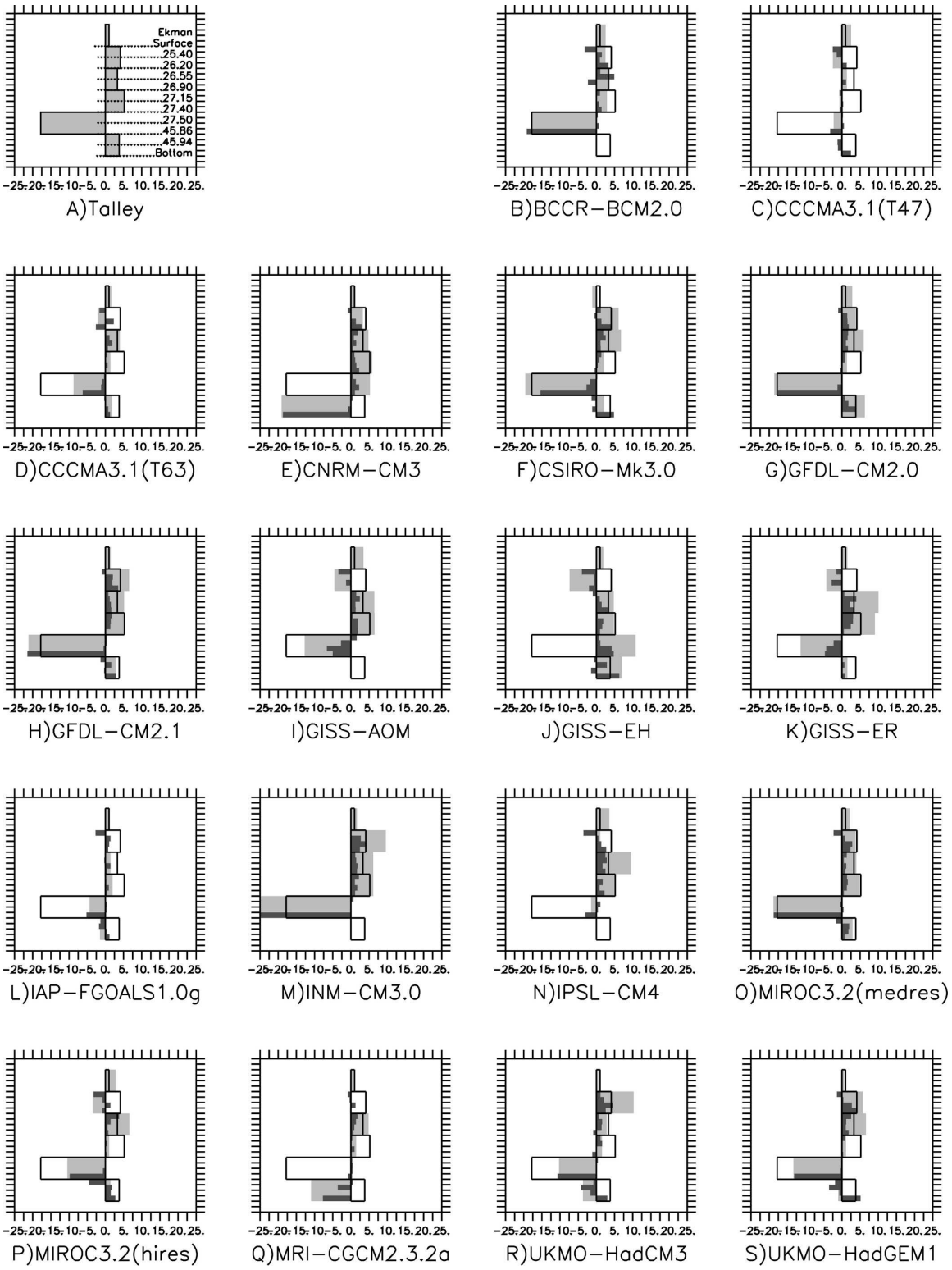

FIG. 5. Inverse transport calculations across 32°S in the Atlantic (between 60°W and 20°E) based on the layer definitions in Talley (2003). The comparison with Talley (2003) assumes that the model's NADW characteristics are similar to those observed in the real ocean, however, in some cases this leads to a somewhat incomplete representation of the computed transports from the model simulation. The pale gray bars are the integrated totals for each layer and can be compared to the black lines, which are the observed values from Talley (2003). The dark gray bars are approximately equal subdivisions of each layer. The Ekman layer transport is calculated from the wind stress and is subtracted from the uppermost layer transport. Positive values are northward transport (Sv).

The salinity structure along 30°W in the Atlantic shows most of the major oceanic water masses. Relatively high salinity (>34.75) North Atlantic Deep Water is observed to be filling the basin between 1500 and 4000 m (Fig. 6). Also seen are the intermediate salinity bottom waters flowing northward and the low salinity (<34.5) Antarctic Intermediate Water subducting at 45°S and moving northward at ~800 m, along with the salty subtropical gyres and the Mediterranean outflow (at 30°N at 1000 m). Separation of the models into the overstable, understable, and "about right" classes is easiest here. The CCCMA(T47), CSIRO, GISS-EH, and MRI have positive salinity anomalies at the surface of the Southern Ocean overlying negative anomalies at depth; all these models are understable (too unstable). The BCCR, INM, IPSL, and UKMO-HadCM3 results also show clear indications of too-light water above and too-dense water below, signs of overstability. The two GFDL simulations, CCCMA(T63), MRI, and UKMO-HadGEM1 runs seem to occupy the middle ground, although even these models suffer from having a too-fresh layer near the surface, with a too-salty layer near 1 km.

As was seen in the salinity errors, the temperature errors at 30°W shown in Fig. 7 also reveal overstable, understable, and neutral simulations. Cold anomalies over warm anomalies are the mark of understability and are seen in the Southern Ocean in BCCR, CNRM, INM, and MIROC(hires). CCCMA(T47), CSIRO, MRI, and the GISS models are all overstable with warm anomalies over cold. The most neutral models (in temperature) are CCCMA(T63) and the GFDL and UKMO models.

The primary process identified here by which the oceanic simulation in a coupled model can affect the ACC is the salinity export of NADW into the Southern Ocean that upwells on the Antarctic side of the current. Table 2 presents several indicators relating to the formation and export of NADW in each of the IPCC models discussed in this study. We find that the models with the best overall ACC transports and Southern Ocean water masses are those in which the outflow of NADW across 30°S is both strong (>14 Sv) and saline (>34.85), like the GFDL runs and the MIROC(medres) run. Several models have strong overturning in the North Atlantic that is not carried into the Southern Ocean (CNRM, IPSL, MRI, and the GISS simulations). NADW is warmer than recycled CDW, so models with a strong southward flow combined with a weak heat transport have too much bottom water in the NADW outflow layers [the CSIRO and MIROC(hires) models]. Also those models with warm anomalies at depth (BCCR, CNRM, INM, and IPSL) tend to have weaker ACC transports as the warmer deep water is upwelled to the surface near Antarctica, reducing the horizontal density gradient. While the UKMO-HadCM3 simulation has reasonable salt export, heat export, and wind strength, the ACC is overly strong because of the major negative salinity anomalies on the north side of the current (Fig. 4b).

The range of seasonal change in area-integrated sea ice cover for each of the models is also included in Table 2 as a measure of the net seasonal impact of brine exclusion due to the formation of ice. There is a wide disparity between the models in their representation of the sea ice cover. The INM-CM3.0, BCCR-BCM2.0, and CSIRO-Mk3.0 results are closest to the observations for the seasonal range of ice cover (from Taylor et al. 2000). INM-CM3.0 and MRI-CGCM2.3.2a have the best representations of the zonally averaged latitudinal sea ice cover (not shown). The IAP-FGOALS1.0g model has nearly permanent, total ice cover out to 60°S and is also the coldest model south of 60°S (see Fig. 4a). IAP, along with the CCCMA runs, the CSIRO, and the MIROC(hires), overestimates the ice cover north 65°S, while the other models tend to underestimate the sea ice cover south of that latitude.

5. Discussion

Assessing the performance of coupled models in the context of the ACC transport is complex, encompassing performance issues from the atmosphere, ice, and ocean components of the models. Returning to the relationships between the ACC transport and the wind stress, temperature gradient, and salinity gradient in Fig. 2, we find that the most important gauges for assessing the likely Southern Ocean simulation performance, in descending order of importance, are 1) the strength of the westerly wind over the Drake Passage latitude band, 2) the air–sea heat flux gradient over the same latitude band (although this quantity is relatively well simulated by the models presented here and therefore introduces little of the model differences presented here), and 3) the salinity gradient across the ACC throughout the water column. This gradient in some models is strongly influenced by variations in surface freshwater flux. However when all the models are considered and based on our understanding of the observations, the salinity gradient seems largely determined by the rate and salinity of North Atlantic Deep Water upwelled on the poleward side of the ACC.

Of these three criteria, the atmospheric components of the models have a larger impact on the simulation of the winds and the gradient in surface heat flux across the current. The ocean components of the coupled

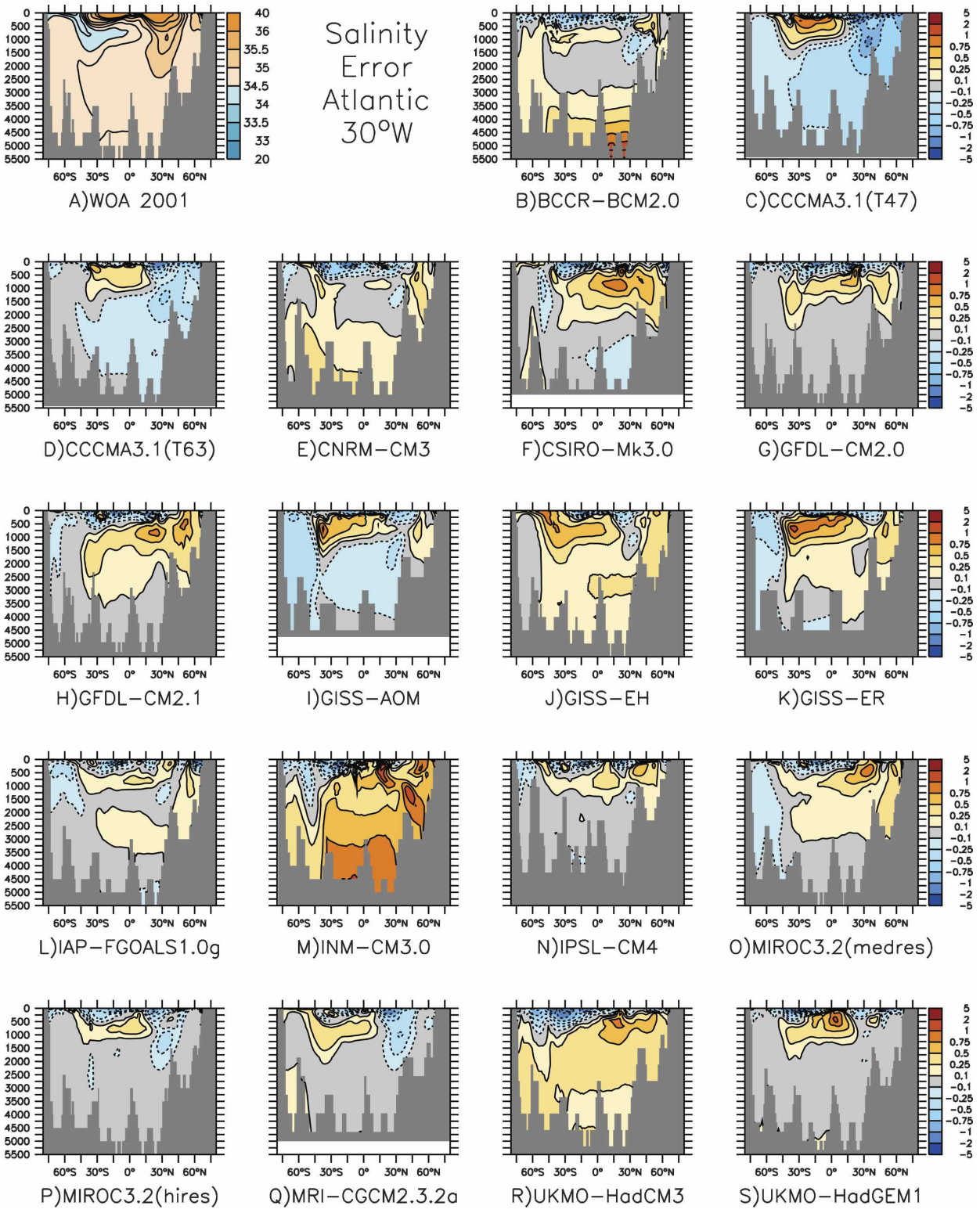

FIG. 6. Salinity differences from (a) the observations along 30°W from 18 of the IPCC ocean models. Positive values indicate the model is more saline than observed.

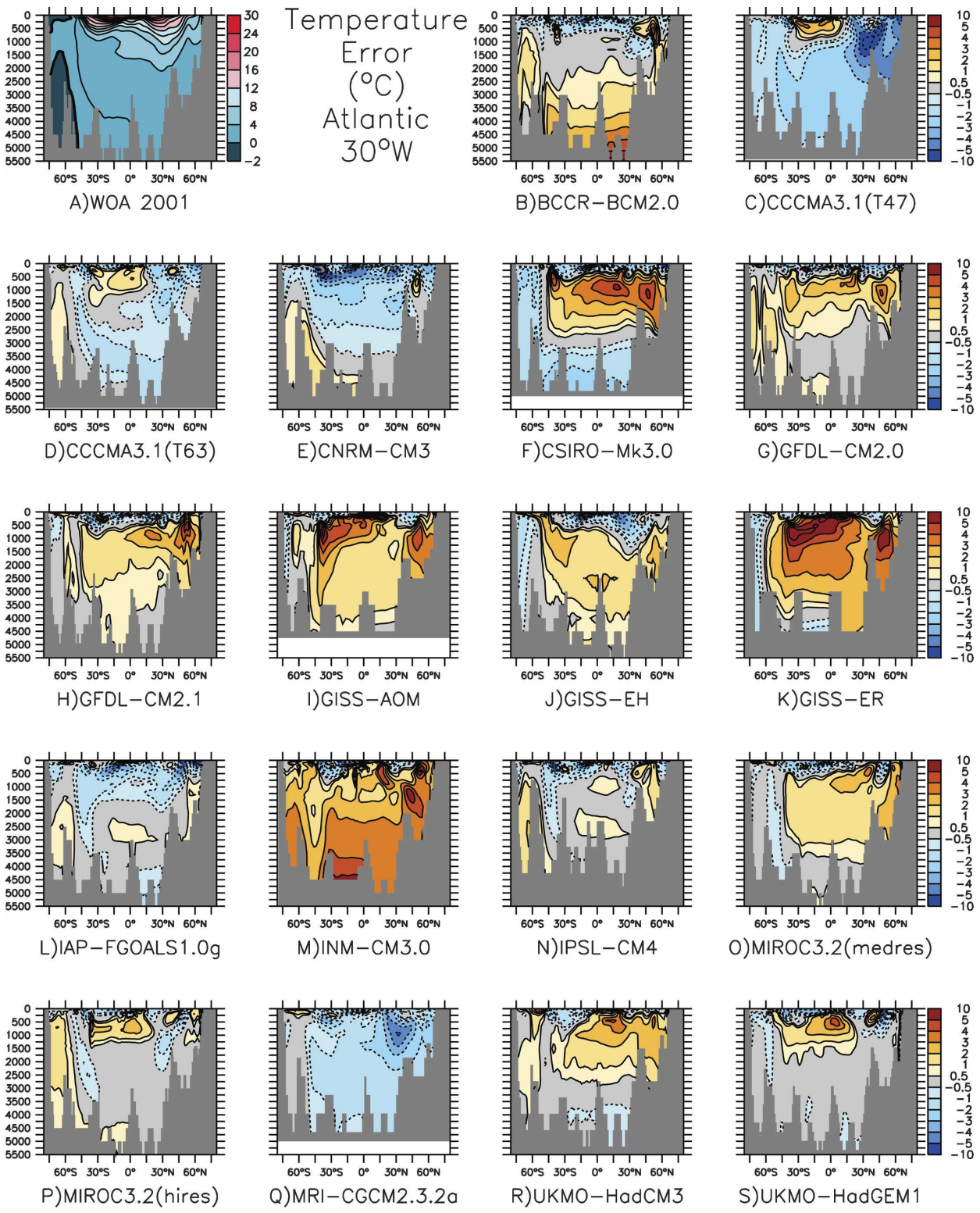

FIG. 7. Temperature differences from (a) the observations along 30°W from 18 of the IPCC ocean models. Positive values indicate the model is warmer than observed.

TABLE 2. Various parameters related to the strength of NADW formation and export. NADW values are from Schmitz (1996). Heat export values for the NADW layer are calculated as temperature transfer (in petawatts where volume is not conserved, PWT) as defined by Talley (2003). Sea ice values are from Taylor et al. (2000). NA indicates data not archived at PCMDI.

Model	ACC (Sv)	Max. NAOT (Sv)	Talley NADW at 30°S (Sv)	Salinity of Talley NADW	Talley NADW salt export (10^6 kg)	Talley NADW heat export (PWT)	Sea ice range (10^{12} m^2)
Observational estimate	135	15–20	15–20				13.6
CSIRO-Mk3.0	336	15.7	12.0	34.84	420	0.23	14.7
GISS-ER	266	36.8	2.3	34.96	80	0.06	11.9
UKMO-HadCM3	223	22.1	13.9	35.01	490	0.26	17.3
GISS-AOM	202	29.1	0.7	34.72	23	0.01	10.7
UKMO-HadGEM1	199	16.3	19.6	34.83	683	0.26	16.0
MIROC3.2(medres)	190	18.7	14.4	34.88	506	0.27	10.6
GFDL-CM2.1	135	24.3	23.3	34.97	818	0.41	15.3
MIROC3.2(hires)	125	13.2	13.5	34.72	470	0.15	16.7
GFDL-CM2.0	113	16.0	18.8	34.92	657	0.33	17.0
CCCMA-CGCM3.1(T63)	106	6.4	6.4	34.68	224	0.09	18.9
BCCR-BCM2.0	105	15.3	19.2	34.88	671	0.30	13.2
MRI-CGCM2.3.2a	94	11.3	4.7	34.83	162	0.04	15.2
CCCMA-CGCM3.1(T47)	93	5.4	1.7	34.57	59	0.01	16.0
INM-CM3.0	80	21.2	11.3	35.42	402	0.30	14.3
IAP-FGOALS1.0g	75	11.1	8.2	34.84	287	0.09	11.2
CNRM-CM3	54	26.4	9.8	34.93	342	0.09	16.2
IPSL-CM4	34	12.4	1.6	34.81	57	0.02	16.4
GISS-EH	−6	39.7	1.4	34.89	50	0.01	NA

models seem to largely determine the rate and salinity of NADW supplied to the Southern Ocean. In most models there is a significant disconnect between the rate of overturning in the North Atlantic and the amount of NADW-like water that is exported from the Atlantic into the Southern Ocean at 30°S (Table 2). The best simulations of the strength and water mass characteristics of the ACC have a strong connection between the formation rate and the export rate of NADW in the South Atlantic (see Table 2).

Based on the analysis presented here, we find that we can divide the Southern Ocean simulations produced by the 18 models into five different classes. While these classes are derived from the IPCC AR4 model simulations of preindustrial climate, we think they have a broader application. It is possible that some past (and future) climates may fall into these broad categories.

1) To fall into the first simulation class, the about right for the present-day climate scenario, a model must simulate the strength and position of the Antarctic Circumpolar for approximately the right reasons. The model must correctly simulate the magnitude and position of Southern Hemisphere westerly winds and the magnitude and distribution of heat and freshwater fluxes, as well as the heat and salt transport into the Southern Ocean associated with NADW. The GFDL-CM2.1 experiment falls solidly into this category. It has its peak winds close to the observed latitude and a reasonable wind stress over the Southern Ocean, fed with the right amount and properties of NADW, resulting in near-observed ACC transport. The MIROC3.2(hires) is also mostly in this class, although it has slightly stronger winds shifted slightly equatorward and its ACC strength is well on the high side of the observations.
2) This class of Southern Ocean simulation falls short of the first classification primarily because of large wind stress errors over the ACC that lead to incorrect ACC transports.
   (a) The excessive wind stress over the ACC leads to a too-strong ACC. The too-strong transport occurs for two reasons, the mechanical force imparted by the wind, and the excessive upwelling of saline NADW along the southern edge of the ACC. The CSIRO-Mk3.0, MIROC3.2(medres), and UKMO-HadGEM1 simulations fall into this category (Figs. 1 and 3).
   (b) This class is the opposite of 2a; weak westerly winds produce a weak ACC (CNRM and IAP). Both the weak mechanical forces imparted by the wind and the too-fresh waters south of the ACC lead to too-weak ACC transport.
3) The third class of Southern Ocean simulation is characterized by an equatorward displacement of

the peak wind stress over the Southern Ocean relative to observations while maintaining relatively strong winds over the channel (too-strong winds, too far north). The strong winds drive strong subtropical gyres and boundary currents like the east Australia Current and the Agulhas Current, which inject both heat and salt into the surface waters on the north side of the ACC in the southwestern corners of the basins. This weakens the density gradient across the channel and thus the ACC. The MIROC3.2(hires) simulation suffers from this shortcoming as do the GFDL-CM2.0, BCCR-BCM2.0, MRI-CGCM2.3.2a, and both CCCMA models.

4) In the fourth class of simulation, an equatorward wind shift is accompanied by weak winds over the channel. In this case, the injection of heat and salt from the subtropics into the Southern Ocean is substantially reduced and the Southern Ocean is dominated by very cold water adjacent to Antarctica; a very strong thermal gradient exists across the current, producing an excessively strong ACC. This regime reminds us of what was typical of simulations obtained from ocean-only models under restoring boundary conditions many years ago, when ocean-only models were often forced with the Hellerman and Rosenstein (1983, hereafter HR83) wind climatology (see Bryan and Lewis 1979 as an example). HR83 is known to be too weak and too equatorward (Harrison 1989), and the use of restoring boundary conditions at the surface keeps the Polar and Subantarctic Fronts near their observed locations, allowing cold water to collect on the south side of the ACC. The GISS-AOM and GISS-ER models are typical of this class.
5) The fifth categorization criterion is related to the formation rate and density of the model's NADW.
   (a) If NADW is excessively weak, fresh, or warm, then it will not cross into the Southern Ocean below the sill depth of the Drake Passage topographic features and upwell on the southern side of the ACC as in the observations. Weak and/or shallow NADW leads to a too-weak eastward ACC transport as the density gradient across the current is smaller than observed (all other things being equal). The GISS-EH, INM-CM3.0, and IPSL-CM4 simulations fall into this class (Table 2). NADW in the INM-CM3.0 simulation is moderately vigorous but very warm, weakening the density gradient across the ACC, which leads to a weaker ACC.
   (b) Conversely, too-large southward NADW export below sill depth will lead to an exaggerated ACC as the saline NADW greatly increases the density of water adjacent to the Antarctic coast. Although the UKMO-HadCM3 simulation does have an exaggerated salinity gradient across the ACC and could fit in this category of simulation (see Fig. 4), the salinity gradient is largely the result of a surface subtropical freshwater bias, rather than an excessive NADW upwelling component.

6. Conclusions

The quality of a coupled climate model's Southern Ocean simulation depends upon both its atmospheric and ocean model components. These two model components influence each other in ways evident in the coupled system's air–sea momentum and buoyancy fluxes, and in the resulting three-dimensional Southern Ocean circulation. Away from the surface, in the ocean interior, the mixing of different water masses largely determines the properties of the water that is upwelled to the surface at a rate that in turn is influenced by winds. And since air–sea heat fluxes over the vast Southern Ocean impact the surface climate within and beyond the Southern Ocean region, a global coupled model's Southern Ocean simulation affects the model's mean climate as well as its response to transient forcings, such as those associated with climate change scenarios. With so many interconnected pieces, it is a challenge to get the Southern Ocean "right" in a global coupled climate model.

In the set of coupled climate models presented here, we find that the most important gauges for assessing the likely Southern Ocean simulation performance, in descending order of importance, are 1) the strength of the westerly wind over the Drake Passage latitude band, 2) the heat flux gradient over the same latitude band (although this quantity seems to be relatively well simulated by the models presented here—as well as can be determined from the observations—and therefore explains little of the intermodel differences presented here), and 3) the salinity gradient across the ACC throughout the water column. This gradient is affected by variations in surface freshwater flux, but it seems largely determined by the rate and salinity of North Atlantic Deep Water upwelled on the poleward side of the ACC. Additional factors found to influence some Southern Ocean simulations include the latitudinal location of the westerly winds.

Based upon these criteria, a framework for categorizing a model's Southern Ocean simulation has been developed and applied to a set of coupled climate mod-

els associated with the forthcoming IPCC Fourth Assessment Report. Only 1 of the 18 models examined is found to have a Southern Ocean simulation that is not considerably deficient with regard to at least one of the criteria used in this study. Even in this "best" model, there are relatively large errors in the simulated variables. The other models are categorized according to which of the criteria they fail to meet, providing information about how and why those model's Southern Ocean simulations differ markedly from observations.

Increasing ocean stratification associated with global warming has been posited to serve as a positive feedback on global warming, reducing the oceanic uptake of anthropogenic carbon dioxide. Previous model results suggest that both the warming associated with anthropogenic CO_2 increase and the increased hydrological cycle could lead to a reduced oceanic uptake of anthropogenic CO_2 in the Southern Ocean, assuming small changes in biological activity. We expect that the differences in the Southern Ocean control climates indicated here will impact these models' responses to changes in radiative forcing with respect to heat and carbon dioxide uptake. This is the subject of a subsequent study.

Acknowledgments. We acknowledge the international modeling groups for providing their data for analysis, the Program for Climate Model Diagnosis and Intercomparison (PCMDI) for collecting and archiving the model data, the JSC/CLIVAR Working Group on Coupled Modeling (WGCM) and their Coupled Model Intercomparison Project (CMIP) and Climate Simulation Panel for organizing the model data analysis activity, and the IPCC WG1 TSU for technical support. The IPCC Data Archive at Lawrence Livermore National Laboratory is supported by the Office of Science, U.S. Department of Energy. We thank Anand Gnanadesikan, Mike Winton, Gary Russell, Gavin Schmidt, and three anonymous reviewers for their thoughtful reviews and discussions.

REFERENCES

Bryan, K., and L. J. Lewis, 1979: A water mass model of the world ocean. *J. Geophys. Res.,* **84** (C5), 2503–2517.

Conkright, M. E., R. A. Locarnini, H. E. Garcia, T. D. O'Brien, T. P. Boyer, C. Stephens, and J. I. Antonov, 2002: World Ocean Atlas 2001: Objective analyses, data statistics, and figures: CD-ROM documentation. National Oceanographic Data Center, Silver Spring, MD, 17 pp.

Cubasch, U., and Coauthors, 2001: Projections of future climate change. *Climate Change 2001: The Scientific Basis,* J. T. Houghton et al., Eds., Cambridge University Press, 526–582.

Cunningham, S. A., S. G. Alderson, B. A. King, and M. A. Brandon, 2003: Transport and variability of the Antarctic Circumpolar Current in Drake Passage. *J. Geophys. Res.,* **108,** 8084, doi:10.1029/2001JC001147.

da Silva, A. M., C. C. Young, and S. Levitus, 1994: *Algorithms and Procedures.* Vol. 1, *Atlas of Surface Marine Data 1994,* NOAA Atlas NESDIS 6, 83 pp.

Fu, L.-L., E. Christensen, M. Lefebvre, and Y. Menard, 1994: TOPEX/POSEIDON mission overview. *J. Geophys. Res.,* **99,** 24 369–24 381.

García, M. A., I. Bladé, A. Cruzado, Z. Velásquez, H. García, J. Puigdefàbregas, and J. Sospedra, 2002: Observed variability of water properties and transports on the World Ocean Circulation Experiment SR1b section across the Antarctic Circumpolar Current. *J. Geophys. Res.,* **107,** 3162, doi:10.1029/2000JC000277.

Gent, P. R., W. G. Large, and F. O. Bryan, 2001: What sets the mean transport through Drake Passage? *J. Geophys. Res.,* **106,** 2693–2712.

Gille, S. T., 1997: The Southern Ocean momentum balance: Evidence for topographic effects from numerical model output and altimeter data. *J. Phys. Oceanogr.,* **27,** 2219–2232.

Gnanadesikan, A., and R. Hallberg, 2000: On the relationship of the circumpolar current to Southern Hemisphere winds in large-scale ocean models. *J. Phys. Oceanogr.,* **30,** 2013–2034.

Gordon, A. L., 1971: Oceanography of Antarctic waters. *Antarctic Oceanology I,* J. L. Reid, Ed., Antarctic Research Series, Amer. Geophys. Union, 169–203.

Gregory, J. M., H. T. Banks, P. A. Stott, J. A. Lowe, and M. D. Palmer, 2004: Simulated and observed decadal variability in ocean heat content. *Geophys. Res. Lett.,* **31,** L15312, doi:10.1029/2004GL020258.

Harrison, D. E., 1989: On climatological monthly mean wind stress and wind stress curl fields over the World Ocean. *J. Climate,* **2,** 57–70.

Hasumi, H., 2002: Modeling the global thermohaline circulation. *J. Oceanogr.,* **58,** 25–33.

Hellerman, S., and M. Rosenstein, 1983: Normal monthly wind stress over the world ocean with error estimates. *J. Phys. Oceanogr.,* **13,** 1093–1104.

Kistler, R., and Coauthors, 2001: The NCEP-NCAR 50-Year Reanalysis: Monthly means CD-ROM and documentation. *Bull. Amer. Meteor. Soc.,* **82,** 247–268.

Manabe, S., R. J. Stouffer, M. J. Spelman, and K. Bryan, 1991: Transient responses of a coupled ocean–atmosphere model to gradual changes of atmospheric CO_2. Part I: Annual mean response. *J. Climate,* **4,** 785–818.

McCartney, M. S., 1977: Subantarctic Mode Water. *A Voyage of Discovery: George Deacon 70th Anniversary Volume,* M. V. Angel, Ed., Pergamon, 103–119.

——, 1982: The subtropical recirculation of Mode Waters. *J. Mar. Res.,* **40** (Suppl.), 427–464.

Munk, W. H., and E. Palmen, 1951: Note on the dynamics of the Antarctic Circumpolar Current. *Tellus,* **3,** 53–55.

Peterson, R. G., and T. Whitworth III, 1989: The subantarctic and polar fronts in relation to deep water masses through the southwestern Atlantic. *J. Geophys. Res.,* **94,** 10 817–10 838.

Sarmiento, J. L., T. M. C. Hughes, R. J. Stouffer, and S. Manabe, 1998: Simulated response of the ocean carbon cycle to anthropogenic climate warming. *Nature,* **393**, 245–249.

Schmitz, W. J., 1996: On the World Ocean circulation: Volume I, some global features/North Atlantic circulation. Woods Hole Oceanographic Institution Tech. Rep. WHOI-96-03, 141 pp.

Schulman, E. E., 1975: A study of topographic effects. *Numerical Models of Ocean Circulation,* National Academy of Science, 147–165.

Stevens, D. P., and V. O. Ivchenko, 1997: The zonal momentum balance in an eddy resolving general circulation model of the Southern Ocean. *Quart. J. Roy. Meteor. Soc.,* **123,** 929–951.

Stommel, H., 1957: A survey of ocean current theory. *Deep-Sea Res.,* **4,** 149–184.

Talley, L. D., 1996: Antarctic Intermediate Water in the South Atlantic. *The South Atlantic: Present and Past Circulation,* G. Wefer et al., Eds., Springer-Verlag, 219–238.

——, 2003: Shallow, intermediate and deep overturning components of the global heat budget. *J. Phys. Oceanogr.,* **33,** 530–560.

Taylor, K. E., D. Williamson, and F. Zwiers, 2000: The sea surface temperature and sea-ice concentration boundary conditions for AMIP II simulations. Tech. Rep. 60, Program for Climate Model Diagnosis and Intercomparison, Lawrence Livermore National Laboratory, 25 pp.